Published in IET Electric Power Applications
Received on 5th May 2009
Revised on 29th July 2009
doi: 10.1049/iet-epa.2009.0101

ISSN 1751-8660

Discriminating broken rotor bar from oscillating load effects using the instantaneous active and reactive powers

C.H. De Angelo[1,2] *G.R. Bossio*[1,2] *G.O. García*[1,2]

[1]*Consejo Nacional de Investigaciones Cientificas y Técnicas (CONICET), Argentina*
[2]*Grupo de Electrónica Aplicada (GEA), Facultad de Ingeniería, UNRC, Ruta Nacional #36 Km. 601, X5804BYA, Río Cuarto, Argentina*
E-mail: cdeangelo@ieee.org

Abstract: A new strategy for detection and diagnosis of broken bars and load oscillations is proposed. The proposed technique is based on the analysis of the instantaneous active and reactive powers spectra, and allows the correct distinction between broken rotor bars and low-frequency load oscillations. A suitable fault severity factor is also proposed, which allows the broken rotor bar fault quantification, while being practically independent of the motor load. By using the proposed technique, a broken bar fault can be detected and diagnosed, even in the presence of load oscillations at frequencies next to twice the slip frequency. Extensive experimental results, both from laboratory and industrial cases, validate the proposal.

1 Introduction

Condition monitoring of rotating electrical machines has been one of the most important research topics in the last decades. Several techniques have been proposed and many of them are currently used in the industry [1]. In particular, condition monitoring based on electrical measurements has received a great interest in the last years since, in most cases, it does not require extra sensors. Also, these techniques are very suitable for on-line monitoring and diagnosis, even in machines where other sensors cannot be installed [2–4].

From all the possible faults on induction motors (IMs), the problem of broken rotor bars has been studied for a long time [5]. Several techniques based on the measurement of electrical quantities have been proposed for broken rotor bar detection and diagnosis [6–8]. The most accepted technique is the so-called motor current signature analysis (MCSA), which consists in the analysis of specific spectrum components of the stator currents, related to certain motor faults. In particular, broken rotor bars are detected by monitoring current spectral components, which appear as sidebands around the supply frequency, at twice the slip frequency and its multiples [3, 9]. The amplitudes of these sidebands are related to the number of broken bars and to the motor load.

However, a low-frequency oscillating load torque affects the stator currents in a similar way as the broken bars do [10], that is, low-frequency sidebands appear around the fundamental frequency. Such torque oscillations could be produced either by the load characteristics (e.g. a reciprocating compressor) or by an abnormal load condition (e.g. load unbalance, misalignment, gearbox fault) [11]. If the frequency of the load torque oscillation is close to twice the slip frequency, it can be confused with a broken bar fault or, at least, obscure the broken bar detection [12], leading to an incorrect diagnosis.

Besides the stator current spectrum, several other techniques have been proposed using the instantaneous power [13], the instantaneous phase [14], the Park vector [15] or the swing angle [16] for broken rotor bar detection, among others. All these techniques use the twice slip frequency component ($2sf$) for detecting broken rotor bars. Thus, a low-frequency oscillating load torque can also affect these strategies.

A similar problem occurs when trying to separate the effects of rotor eccentricities and load oscillations at the rotor frequency. Some strategies have been proposed to eliminate the effects of oscillating loads in rotor eccentricity diagnosis. A model reference-based strategy was proposed in [17], which needs several motor parameters to obtain a correct separation. Other strategy proposed a rotor fault indicator in a characteristic reference frame for eccentricity diagnosis in the presence of load oscillations [18].

Among other factors, a reliable fault detection and identification strategy must [8]

- produce a quantitative fault detection in order to state an absolute fault threshold;
- be insensitive to operation condition;
- allow a correct fault identification, avoiding false alarms.

With this in mind, a new strategy for detection and diagnosis of broken bar and load oscillations is proposed in this paper. The proposed technique is based on the analysis of the instantaneous active and reactive powers spectra, and allows distinguishing between broken rotor bars and low-frequency load oscillations correctly. A complete theoretical analysis of the effects of broken rotor bars and oscillating loads over the instantaneous active and reactive powers is developed. This analysis is validated through the use of a multiple-coupled circuits model. A suitable fault severity factor is also proposed, which allows the broken rotor bar fault quantification, while being practically independent of the motor load. By using the proposed technique, a broken bar fault can be detected and diagnosed, even in the presence of load oscillations at frequencies next to twice the slip frequency. Extensive experimental results, both from laboratory and industrial cases, validate the proposal.

2 Effects of broken bars and load oscillations on the stator currents

As stated above, broken rotor bars and oscillating loads produce similar effects on the stator currents. In [9], a detailed analysis of the stator current components introduced by broken bars was presented, including the effect of the speed ripple. Following the same procedure, the current sidebands produced by oscillating load torque can be obtained.

Broken rotor bars produce a backward-rotating field, because of the rotor asymmetry. This rotating field induces electromotive force (EMF) and stator current components with a frequency of $(1-2s)f$, where f is the stator frequency and s is the slip. This component is referred to as the lower twice slip frequency sideband, and its amplitude depends on the rotor asymmetry and the motor load level.

According to [9], this sideband component can be expressed in complex space vector form as

$$\boldsymbol{i}_1' = \sqrt{3} I_1' \mathrm{e}^{j[(1-2s)\omega t - \alpha_1]} \tag{1}$$

where I_1' is the rms value of the lower sideband component, α_1 is its angular displacement and ω is the supply angular frequency.

A torque oscillation at twice the slip frequency is produced when the sideband current interacts with the fundamental magnetic flux

$$\Delta T_1' = -3PI_1'\Psi \sin(2s\omega t + \alpha_1 - \alpha_\psi) \tag{2}$$

with Ψ being the rms value of the fundamental flux and α_ψ its angular displacement.

By defining the torque oscillation angle as $\alpha_T = \alpha_1 - \alpha_\psi$, the oscillating torque can be expressed as follows

$$\Delta T_1' = -3PI_1'\Psi \sin(2s\omega t + \alpha_T) \tag{3}$$

Then, by following the procedure described in [9], the two sidebands produced by the rotor asymmetry are obtained.

- *Upper sideband*

$$\boldsymbol{i}_r = \sqrt{3} I_r \mathrm{e}^{j[(1+2s)\omega t + \alpha_T - \alpha_\psi + (\pi/2) - \alpha_s]} \tag{4}$$

with $I_r = [(1+2s)\omega](kPI_1'\Psi/2Z_s)$.

- *Lower sideband*

$$\boldsymbol{i}_1 = \boldsymbol{i}_1' + \boldsymbol{i}_1'' = \sqrt{3} I_1' \mathrm{e}^{j[(1-2s)\omega t - \alpha_1]} + \sqrt{3} I_1'' \mathrm{e}^{j[(1-2s)\omega t - \alpha_T - \alpha_\psi - (\pi/2) - \alpha_s]} \tag{5}$$

with $I_1'' = [(1-2s)\omega](kPI_1'\Psi/2Z_s)$.

Here, $k = (3P\Psi/J4s^2\omega^2)$, $\boldsymbol{Z}_s = Z_s \mathrm{e}^{j\alpha_s}$ is the stator impedance, J is the motor-load inertia and P is the pole pair number.

These expressions allow the analysis of the effects of the rotor asymmetry over the stator currents, including the effects of the speed ripple, produced by this asymmetry. As can be seen, the lower sideband is produced by two causes: the rotor asymmetry and the speed ripple. However, the upper sideband is produced only by the speed ripple.

A similar procedure can be used for the study of the effects of a load oscillating at $\omega_L \ll \omega$. In such a case, the component produced by the rotor asymmetry does not exist, and the sideband's magnitude can be calculated starting from (3), where the magnitude of the oscillating torque (T_p) will be given by the load characteristics.

IET Electr. Power Appl., 2010, Vol. 4, Iss. 4, pp. 281–290
doi: 10.1049/iet-epa.2009.0101

- *Upper sideband*

$$\boldsymbol{i}_{\mathrm{r}} = \sqrt{3} I_{\mathrm{r}} \mathrm{e}^{j[(\omega+\omega_{\mathrm{L}})t+\alpha_{\mathrm{T}}-\alpha_{\psi}+(\pi/2)-\alpha_{\mathrm{s}}]} \tag{6}$$

with $I_{\mathrm{r}} = [(\omega + \omega_{\mathrm{L}})](T_{\mathrm{p}} P \Psi / 2 J \omega_{\mathrm{L}}^2 Z_{\mathrm{s}})$.

- *Lower sideband*

$$\boldsymbol{i}_{\mathrm{l}} = \sqrt{3} I_{\mathrm{l}}'' \mathrm{e}^{j[(\omega-\omega_{\mathrm{L}})t-\alpha_{\mathrm{T}}-\alpha_{\psi}-(\pi/2)-\alpha_{\mathrm{s}}]} \tag{7}$$

with $I_{\mathrm{l}}'' = [(\omega - \omega_{\mathrm{L}})](T_{\mathrm{p}} P \Psi / 2 J \omega_{\mathrm{L}}^2 Z_{\mathrm{s}})$.

Thus, if the frequency of the oscillating load is next to $2sf$, it will be very difficult to distinguish such a case from broken rotor bars. In the next section, the effects of broken bars and oscillating loads over the instantaneous active and reactive power are analysed, and a method to discriminate between them is proposed.

3 Effects of broken bars and load oscillations on the instantaneous powers

The use of instantaneous power for broken bar and mechanical abnormalities detection was previously presented in the literature. The total instantaneous power [19], the reactive power [20] and the phase angle [21] have been proposed and evaluated for broken bars diagnosis. Similar proposals can be found to diagnose rotor eccentricity [22, 23]. However, the possibility of distinguishing between broken bars and low-frequency load oscillations through the instantaneous powers has not been deeply investigated.

As previously stated, the complex vector stator current in the case of broken bars is given by

$$\boldsymbol{i}_{\mathrm{s}} = \sqrt{3} I \mathrm{e}^{j\omega t} + \boldsymbol{i}_{\mathrm{r}} + \boldsymbol{i}_{\mathrm{l}} \tag{8}$$

By considering a sinusoidal supply voltage with magnitude V (rms) and phase φ, the complex vector voltage is

$$\boldsymbol{v}_{\mathrm{s}} = \sqrt{3} V \mathrm{e}^{j(\omega t+\varphi)} \tag{9}$$

and the instantaneous complex power is given by

$$\boldsymbol{s} = \boldsymbol{v}_{\mathrm{s}} \boldsymbol{i}_{\mathrm{s}}^{*} = \sqrt{3} V \mathrm{e}^{j(\omega t+\varphi)} \left[\sqrt{3} I \mathrm{e}^{-j\omega t} + \boldsymbol{i}_{\mathrm{r}}^{*} + \boldsymbol{i}_{\mathrm{l}}^{*} \right] \tag{10}$$

where * stands for the complex conjugate value. By expanding (10), the instantaneous complex power in the case of broken rotor bars results in

$$\begin{aligned} \boldsymbol{s} = {} & 3VI\mathrm{e}^{j\varphi} + 3VI_{\mathrm{r}}\mathrm{e}^{-j[2s\omega t+\alpha_{\mathrm{T}}-\alpha_{\psi}+(\pi/2)-\alpha_{\mathrm{s}}-\varphi]} \\ & + 3VI_{\mathrm{l}}'\mathrm{e}^{j[2s\omega t+\alpha_{\mathrm{l}}+\varphi]} \\ & + 3VI_{\mathrm{l}}''\mathrm{e}^{j[2s\omega t+\alpha_{\mathrm{T}}+\alpha_{\psi}+(\pi/2)+\alpha_{\mathrm{s}}+\varphi]} \end{aligned} \tag{11}$$

This power can be separated into the instantaneous active (real) power, $p(t) = \mathrm{Re}[\boldsymbol{s}]$

$$\begin{aligned} p(t) = {} & 3VI\cos(\varphi) \\ & + 3VI_{\mathrm{r}}\cos\left(2s\omega t + \alpha_{\mathrm{T}} - \alpha_{\psi} + \frac{\pi}{2} - \alpha_{\mathrm{s}} - \varphi\right) \\ & + 3VI_{\mathrm{l}}'\cos(2s\omega t + \alpha_{\mathrm{l}} + \varphi) \\ & + 3VI_{\mathrm{l}}''\cos\left(2s\omega t + \alpha_{\mathrm{T}} + \alpha_{\psi} + \frac{\pi}{2} + \alpha_{\mathrm{s}} + \varphi\right) \end{aligned} \tag{12}$$

and the instantaneous reactive (imaginary) power [24], $q(t) = \mathrm{Im}[\boldsymbol{s}]$

$$\begin{aligned} q(t) = {} & 3VI\sin(\varphi) \\ & - 3VI_{\mathrm{r}}\sin\left(2s\omega t + \alpha_{\mathrm{T}} - \alpha_{\psi} + \frac{\pi}{2} - \alpha_{\mathrm{s}} - \varphi\right) \\ & + 3VI_{\mathrm{l}}'\sin(2s\omega t + \alpha_{\mathrm{l}} + \varphi) \\ & + 3VI_{\mathrm{l}}''\sin\left(2s\omega t + \alpha_{\mathrm{T}} + \alpha_{\psi} + \frac{\pi}{2} + \alpha_{\mathrm{s}} + \varphi\right) \end{aligned} \tag{13}$$

For each power, the first term corresponds to the average power, whereas the remaining three are the oscillating active and reactive powers ($\tilde{p}$, $\tilde{q}$) [25], which has a frequency of $2sf$ for broken rotor bars.

By working with the arguments and grouping terms, the oscillating powers yield

$$\begin{aligned} \tilde{p}(t) = {} & 3VI_{\mathrm{l}}'\cos(2s\omega t + \alpha_{\mathrm{l}} + \varphi) \\ & - 3V(I_{\mathrm{r}} + I_{\mathrm{l}}'')\sin(2s\omega t + \alpha_{\mathrm{T}})\cos(\alpha_{\psi} + \alpha_{\mathrm{s}} + \varphi) \\ & + 3V(I_{\mathrm{r}} - I_{\mathrm{l}}'')\cos(2s\omega t + \alpha_{\mathrm{T}})\sin(\alpha_{\psi} + \alpha_{\mathrm{s}} + \varphi) \end{aligned} \tag{14}$$

$$\begin{aligned} \tilde{q}(t) = {} & 3VI_{\mathrm{l}}'\sin(2s\omega t + \alpha_{\mathrm{l}} + \varphi) \\ & - 3V(I_{\mathrm{r}} - I_{\mathrm{l}}'')\cos(2s\omega t + \alpha_{\mathrm{T}})\cos(\alpha_{\psi} + \alpha_{\mathrm{s}} + \varphi) \\ & - 3V(I_{\mathrm{r}} + I_{\mathrm{l}}'')\sin(2s\omega t + \alpha_{\mathrm{T}})\sin(\alpha_{\psi} + \alpha_{\mathrm{s}} + \varphi) \end{aligned} \tag{15}$$

Now, from the expressions for I_{r} (4) and I_{l}'' (5), if the slip is small, $I_{\mathrm{r}} \simeq I_{\mathrm{l}}''$, and

$$\begin{aligned} \tilde{p}(t) = {} & 3VI_{\mathrm{l}}'\cos(2s\omega t + \alpha_{\mathrm{l}} + \varphi) \\ & - 3VI_{2sb}\sin(2s\omega t + \alpha_{\mathrm{T}})\cos(\alpha_{\psi} + \alpha_{\mathrm{s}} + \varphi) \end{aligned} \tag{16}$$

$$\begin{aligned} \tilde{q}(t) = {} & 3VI_{\mathrm{l}}'\sin(2s\omega t + \alpha_{\mathrm{l}} + \varphi) \\ & - 3VI_{2sb}\sin(2s\omega t + \alpha_{\mathrm{T}})\sin(\alpha_{\psi} + \alpha_{\mathrm{s}} + \varphi) \end{aligned} \tag{17}$$

where $I_{2sb} = I_{\mathrm{r}} + I_{\mathrm{l}}''$.

By replacing $\alpha_1 = \alpha_T + \alpha_\psi$

$$\tilde{p}(t) = 3VI_1' \cos(2s\omega t + \alpha_T + \alpha_\psi + \varphi) - 3VI_{2sb} \sin(2s\omega t + \alpha_T) \cos(\alpha_\psi + \alpha_s + \varphi) \quad (18)$$

$$\tilde{q}(t) = 3VI_1' \sin(2s\omega t + \alpha_T + \alpha_\psi + \varphi) - 3VI_{2sb} \sin(2s\omega t + \alpha_T) \sin(\alpha_\psi + \alpha_s + \varphi) \quad (19)$$

In common motor operating conditions, the angles $\alpha_\psi + \varphi \simeq (\pi/2)$, yielding

$$\tilde{p}(t) = -3V[I_1' - I_{2sb} \sin(\alpha_s)] \sin(2s\omega t + \alpha_T) \quad (20)$$

$$\tilde{q}(t) = 3VI_1' \cos(2s\omega t + \alpha_T) - 3VI_{2sb} \cos(\alpha_s) \sin(2s\omega t + \alpha_T) \quad (21)$$

The oscillating instantaneous reactive power can be further expressed as

$$\tilde{q}(t) = 3V\sqrt{(I_1')^2 + (I_{2sb})^2 \cos^2(\alpha_s)} \cos(2s\omega t + \alpha_T + \zeta) \quad (22)$$

where

$$\zeta = \tan^{-1}\left\{\frac{I_{2sb} \cos(\alpha_s)}{I_1'}\right\}$$

Therefore the magnitudes of the oscillating powers depend on the amplitude of the current sidebands and the angle of the impedance α_s.

Although the preceding analysis is based on a simplified model, some important conclusions can be drawn from (20) and (22). The usual values of α_s indicate that for broken rotor bars, the sidebands produced by the speed ripple counteract the effect of the rotor asymmetry, reducing the amplitude of the oscillating instantaneous active power. On the other hand, the amplitude of the oscillating instantaneous reactive power is practically unaffected by the speed ripple. This effect makes the component of the instantaneous reactive power at $2sf$ much greater than the component of the instantaneous active power at this frequency. Thus, broken rotor bars can be detected by analysing the instantaneous reactive power.

For a more complete analysis of the effects of broken bars over the oscillating instantaneous powers, a more complex model is needed. Thus, the amplitude of the instantaneous active and reactive power components at $2sf$ was calculated for different faults and operating conditions by using a multiple-coupled circuits model of the IM. The breakage of rotor bars was modelled as proposed in [26], and the amplitudes of the oscillating power components are shown in Fig. 1*a* for different number of broken rotor bars (motor data are shown in Table 1). As can be seen, the amplitude of the instantaneous reactive power component grows with the number of broken bars, and its magnitude is almost ten times that of the instantaneous active power. The load dependence of the instantaneous power components is shown in Fig. 1*b*, where it can be appreciated that the oscillating instantaneous reactive power grows with the motor load. Since the oscillating components depend on the speed ripple, the inertia of the motor-load set influences their amplitudes. Fig. 1*c* shows the amplitudes of the oscillating power components as a function of the drive inertia. It must be noted that the difference between the

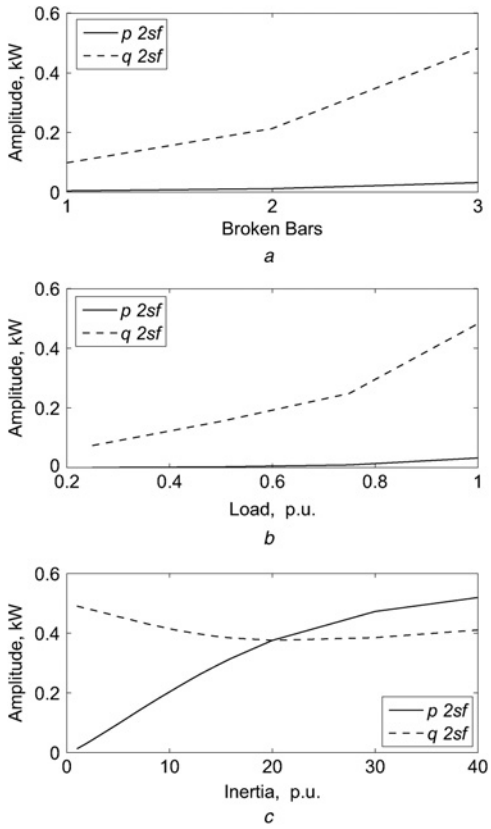

Figure 1 *Oscillating powers at 2sf (simulation results)*
a As a function of the number of broken bars
b As a function of the load
c As a function of the drive inertia

Table 1 Technical data of the IM used for simulations and laboratory experimental results

rated power	5.5 kW
rated voltage	380 V
frequency	50 Hz
rated current	11.1 A
rated speed	1470 rpm
power factor	0.85
number of rotor bars	40
rotor inertia	0.02 kgm^2

IET Electr. Power Appl., 2010, Vol. 4, Iss. 4, pp. 281–290
doi: 10.1049/iet-epa.2009.0101

active and reactive power components is reduced for high motor-inertia values. These results are similar to those obtained by using the simplified equations (20) and (22). On the limit, if infinite inertia is considered, the amplitude of both components will be the same

$$\tilde{p}(t) = -3VI_1' \sin(2s\omega t + \alpha_T) \quad (23)$$

$$\tilde{q}(t) = 3VI_1' \cos(2s\omega t + \alpha_T) \quad (24)$$

By following the same procedure as above for the oscillating load case, the oscillating instantaneous active and reactive powers result in

$$\tilde{p}(t) = 3VI_{2sb} \sin(\alpha_s) \sin(\omega_L t + \alpha_T) \quad (25)$$

$$\tilde{q}(t) = -3VI_{2sb} \cos(\alpha_s) \sin(\omega_L t + \alpha_T) \quad (26)$$

For the usual values of α_s, the oscillating component of the instantaneous reactive power results practically null. Thus, oscillating load torque can be diagnosed through analysing the instantaneous active power.

4 Proposed strategy for broken rotor bars detection

As stated above, the commonly used MCSA does not allow discriminating between a motor with broken rotor bars from a motor driving an oscillating load. To overcome this problem, the analysis of the instantaneous active and reactive powers is proposed in this paper.

First, the low-frequency components of the oscillating instantaneous active and reactive powers are analysed. By comparing the components around the $2sf$ frequency, a case of broken rotor bars can be diagnosed if the amplitude of the instantaneous reactive power component at this frequency is greater than that of the instantaneous active power component.

Second, a broken bar severity factor can be established on the basis of the amplitude of the $2sf$ instantaneous reactive power component. Since the amplitude of this component depends on the motor load, the fault severity factor (SF_q) is defined as the relation between the instantaneous reactive power at $2sf$, $\tilde{q}_{2sf}$ and the average active power, P_{av}

$$SF_q = \frac{\tilde{q}_{2sf}}{P_{av}} \times 100\% \quad (27)$$

This severity factor gives a good approximation to the percentage of contiguous broken bars, while being nearly independent from the motor load state.

5 Experimental validation

The proposed strategy was extensively tested for different fault and load conditions. Several tests were performed in a test bench that allows to reproduce either broken rotor bars or oscillating loads. The results obtained from these tests are presented in this section. Results obtained from some representative industrial cases are also presented.

5.1 Laboratory results

Laboratory results were obtained from a test bench composed by the motor under test, supplied from the grid, coupled to an IM driven by an adjustable speed drive. Two phase currents and two line voltages were measured and registered with an oscillographic recorder. Currents were measured by using AC current probes, whereas line voltages were acquired through 10:1 attenuation isolated voltage probes. For each test, 56 000 samples at 4 kHz sampling frequency were registered. The data were analysed in a personal computer.

The motor under test has several rotors: a healthy one and three rotors with broken bars, ranging from one to three contiguous broken bars. Rotor bar breakage was produced by drilling the bar (Fig. 2). The technical data of this motor are shown in Table 1.

The load of the motor under test is given by a torque-controlled IM drive, which acts as a programmable load. In order to emulate the oscillating load, the reference of this drive is a constant value plus the desired oscillating torque.

The results obtained for a motor with three broken rotor bars (7.5% of the total bars) at 75% constant load are shown in Fig. 3. The frequency spectrum of the stator current is shown in Fig. 3*a*. It can be seen that sideband components at $2sf$ produced by the rotor asymmetry appear around the fundamental component. The amplitude of these sidebands is about 1.8% of the fundamental current. A fault severity factor can be calculated from this spectrum (SF_i), as the sum of the amplitudes of the sidebands, referred to the fundamental current [9], which gives $SF_i = 3.666\%$. This fault severity gives a value of broken bars lower than the actual one, due to the fact that drilling the bars does not produce a complete bar interruption. Also, interlaminar currents may occur, which reduce the fault severity.

The spectrum of the instantaneous active power is shown in Fig. 3*b*, where it can be appreciated that the amplitude

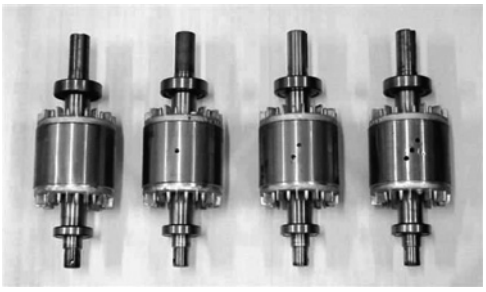

Figure 2 *Rotors used for the experiments*

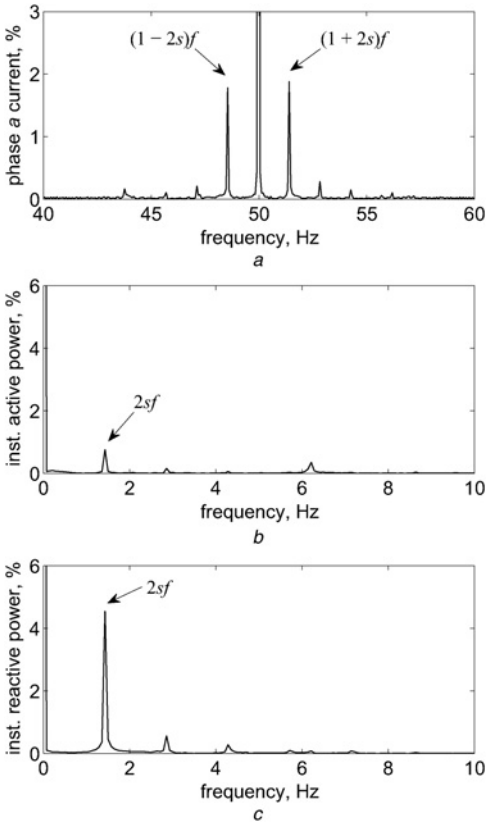

Figure 3 *5.5 kW motor with three broken bars, 75% load*
a Current spectrum ($SF_i = 3.666\%$)
b Instantaneous active power spectrum
c Instantaneous reactive power spectrum ($SF_q = 4.547\%$)

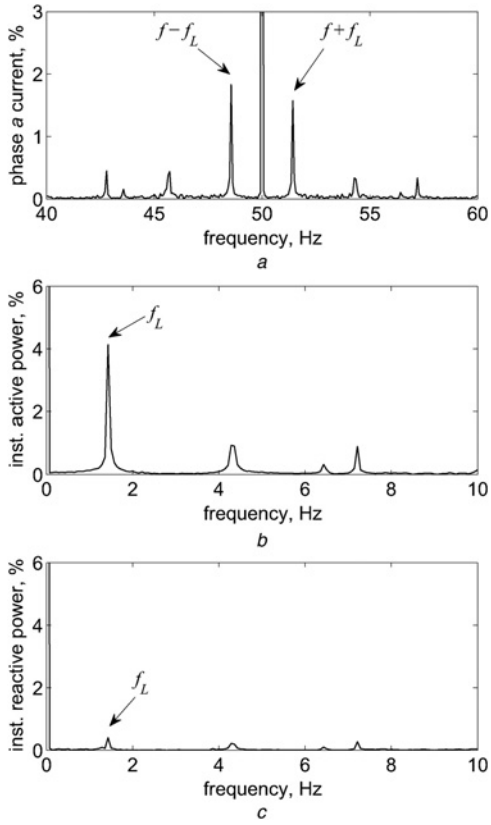

Figure 4 *5.5 kW healthy motor, oscillating load at 1.44 Hz (75% mean value, 3% peak to peak)*
a Current spectrum ($SF_i = 3.405\%$)
b Instantaneous active power spectrum
c Instantaneous reactive power spectrum ($SF_q = 0.398\%$)

of the oscillating power at $2sf$ is less than 1% of the average active power. Fig. 3*c* shows the spectrum of the instantaneous reactive power. This spectrum is referred to the average active power, in order to make the results comparable for any load state. It also makes the proposed severity factor (27) easier to calculate. It can be seen that the amplitude of the $2sf$ component is much greater than the one of the instantaneous active power, and it gives a fault severity factor of $SF_q = 4.547\%$.

The results obtained for the motor with a healthy rotor driving a pulsating load (load torque oscillation at 1.44 Hz, mean value 75%, peak-to-peak value 3% referred to the rated motor torque) are shown in Fig. 4. As can be seen, no difference practically exists between the spectra of Figs. 3*a* and 4*a*. This is due to the fact that the frequency of the oscillating load f_L is close to twice the slip frequency. However, it must be noted that the spectra of the instantaneous active and reactive powers are really different from those of the broken bars case. The oscillating active power clearly reflects the effect of the oscillating load, through the great amplitude of its component at f_L (Fig. 4*b*). On the other hand, the oscillating reactive power is practically negligible (Fig. 4*c*). Morover, the proposed fault severity factor in this case is equal to $SF_q = 0.398\%$, thus being clear that the motor has no broken bars.

Two additional experiments were performed in order to demonstrate the ability of the proposed strategy to decouple the effects of broken bars and load oscillations. First, the motor with three broken rotor bars was loaded with a pulsating load, whose frequency is next to twice the slip frequency (oscillation at 2 Hz, mean value 75%, peak-to-peak value 3% referred to the rated motor torque). The stator current spectrum shows the sidebands at $\pm 2sf$ produced by broken bars, and the sidebands at $\pm f_L$ produced by the oscillating load (Fig. 5*a*). Both effects can be clearly discriminated from the instantaneous powers spectra (Figs. 5*b* and *c*).

In a second experiment, a motor with one broken bar (2.5% of the total bars) was loaded with the same pulsating load torque. The results are shown in Fig. 6, where the correct separation of the two effects can be appreciated in the instantaneous active and reactive power spectra.

An experimental evaluation of the proposed severity factor is shown in Fig. 7. The fault severity factor was obtained for the motor with one, two and three broken bars, at different load conditions. As Fig. 7*a* shows, the proposed severity factor presents a clear difference between different numbers

doi: 10.1049/iet-epa.2009.0101

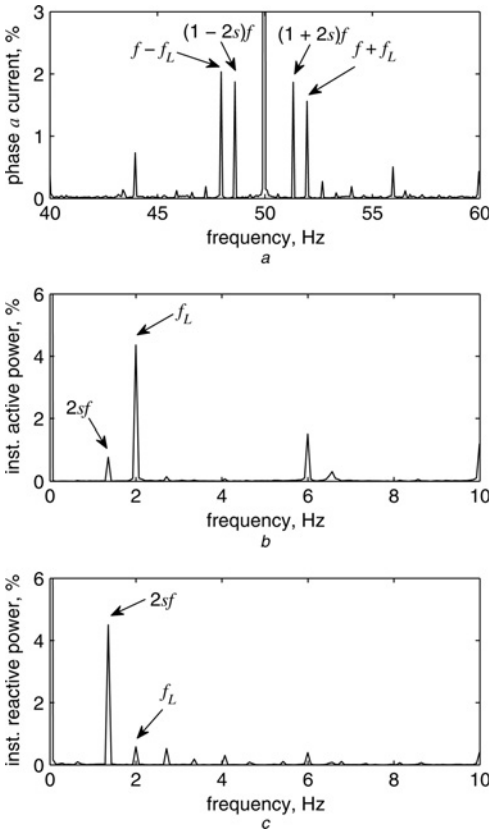

Figure 5 *5.5 kW motor with three broken bars, oscillating load at 2 Hz (75% mean value, 3% peak to peak)*

a Current spectrum ($SF_i = 3.737\%$)
b Instantaneous active power spectrum
c Instantaneous reactive power spectrum ($SF_q = 4.502\%$)

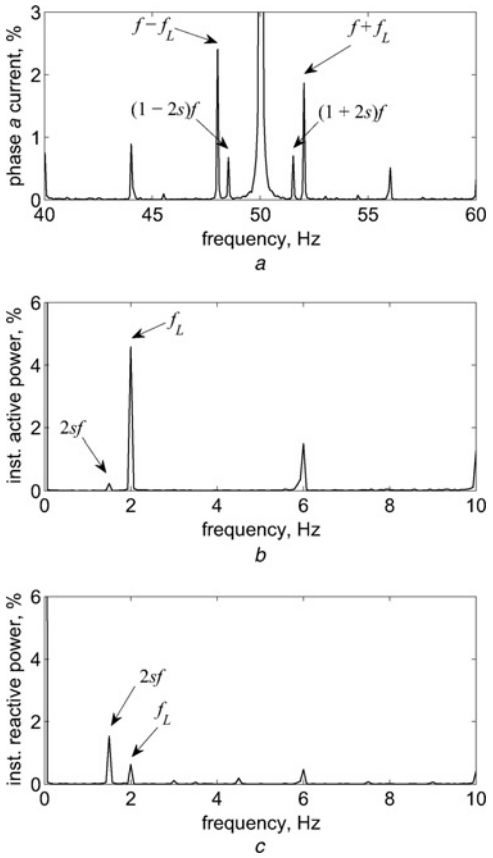

Figure 6 *5.5 kW motor with one broken bar, oscillating load at 2 Hz (75% mean value, 3% peak to peak)*

a Current spectrum ($SF_i = 1.378\%$)
b Instantaneous active power spectrum
c Instantaneous reactive power spectrum ($SF_q = 1.531\%$)

of broken bars, while being almost independent of the load level within the considered operating range. This makes it possible to set a threshold or an alarm level avoiding false alarms. By comparing the proposed severity factor with the one based on the current sidebands amplitude (Fig. 7*b*) [9], it can be seen that the last one does not allow the setting of a threshold independent of the load level.

5.2 Industrial cases

The proposed strategy was also tested on different machines, working in industrial plants. Two industrial cases are presented in this paper: an IM with broken rotor bars and a healthy motor driving an oscillating load.

The results obtained from an IM driving a high-pressure pump, operating at 90% load, are shown in Fig. 8. The nameplate data of this machine are presented in Table 2. In this case, voltages and currents were measured in the secondary of the corresponding voltage and current measurement transformers. The current spectrum (Fig. 8*a*) shows sidebands that can be produced by broken rotor bars. By comparing the instantaneous active and reactive power spectra (Figs. 8*b* and *c*, respectively), it results clear that the motor has a rotor fault. Moreover, the severity of the fault

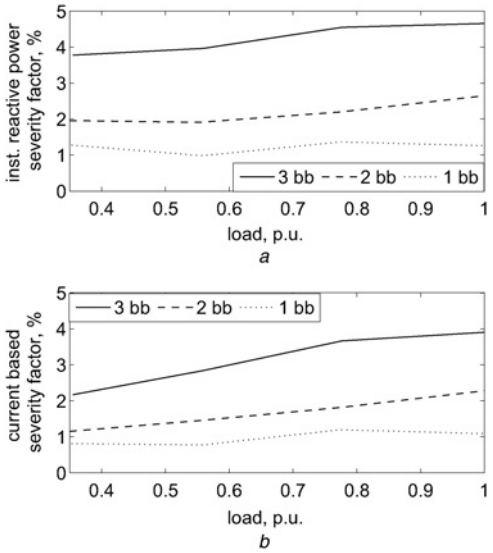

Figure 7 *Severity factors for a 5.5 kW motor with different number of broken bars (bb), as a function of the load level*

a Proposed severity factor
b Current sidebands-based severity factor

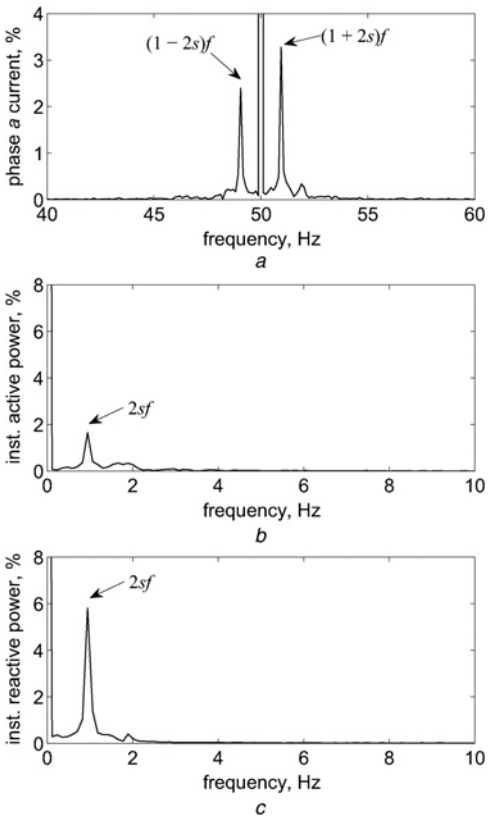

Figure 8 *1656 kW motor driving a high-pressure pump with five broken rotor bars*

a Current spectrum ($SF_i = 5.673\%$)
b Instantaneous active power spectrum
c Instantaneous reactive power spectrum ($SF_q = 5.819\%$)

Table 2 Technical data of the IM-high pressure pump

rated power	1656 kW
rated voltage	2300 V
frequency	50 Hz
rated current	475 A
rated speed	1488 rpm
power factor	0.91
number of rotor bars	76

is about $SF_q = 5.819\%$. In a later inspection, it was verified that the machine had five broken rotor bars, which is about 6.58% of the bars.

Finally, Fig. 9 shows the results obtained for a healthy motor driving the rollers of a flour mill (Table 3). This load is usually constant under normal operating conditions. However, the measurements performed on this motor shows sidebands at ± 4 Hz, which can be confused with broken bars. By applying the proposed strategy, it can be seen that the oscillating active power component is much

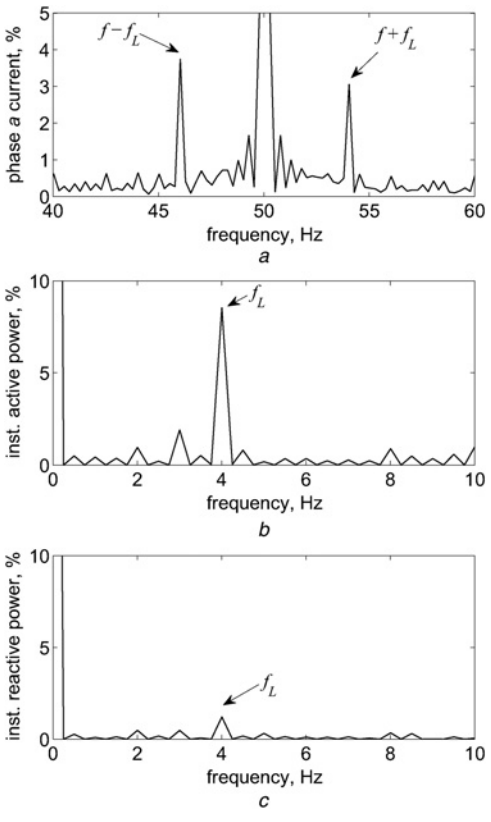

Figure 9 *112 kW motor driving a roller mill*

a Current spectrum
b Instantaneous active power spectrum
c Instantaneous reactive power spectrum

Table 3 Technical data of the IM-roller mill

rated power	112 kW
rated voltage	380 V
frequency	50 Hz
rated current	204 A
rated speed	1485 rpm
power factor	0.82

greater than the oscillating reactive power. This implies a problem related to the load. In this case, the oscillation is produced by a shaft misalignment of one of the reduction stages in the transmission between the motor and the rollers.

All these results demonstrate the capability of the proposed strategy to separate the effect of rotor faults (broken rotor bars) from oscillating or pulsating loads.

6 Discussion and conclusions

The problem of discriminating between the effects of broken rotor bars and low-frequency oscillating loads is arisen in this

doi: 10.1049/iet-epa.2009.0101

paper. A complete analysis based on a simplified model of the effects of broken bars was presented, showing the effects of both broken bars and oscillating load on the instantaneous active and reactive powers. The analysis was complemented through the evaluation of the effects of broken bars under different operation conditions, using a complete motor model.

From such an analysis, a new strategy based on the analysis of the instantaneous active and reactive powers was proposed to distinguish between a broken bar fault and an oscillating load. By analysing the low-frequency components of the instantaneous active and reactive power spectra, it was demonstrated that broken rotor bars mainly affect the instantaneous reactive power, whereas the oscillating load torque affects the instantaneous active power. Thus, broken rotor bars can be diagnosed if the amplitude of the oscillating reactive power at twice the slip frequency is greater than that of the instantaneous active power component.

Moreover, a suitable fault severity factor was proposed based on the amplitude of the $2sf$ component of the instantaneous reactive power referred to the average active power. It was demonstrated that this severity factor is practically independent of the load level.

Extensive experimental validation was presented, showing the effectiveness of the proposal for detecting and diagnosing broken rotor bars even in motors driving oscillating loads.

7 Acknowledgment

This work was supported by Universidad Nacional de Río Cuarto (UNRC), FONCyT-ANPCyT, MinCyT-Cba and CONICET.

8 References

[1] TAVNER P.J.: 'Review of condition monitoring of rotating electrical machines', *IET Electr. Power Appl.*, 2008, **2**, (4), pp. 215–247

[2] NANDI S., TOLIYAT H.A., LI X.: 'Condition monitoring and fault diagnosis of electrical motors – a review', *IEEE Trans. Energy Convers.*, 2005, **20**, (4), pp. 719–729

[3] BENBOUZID M.E.H.: 'A review of induction motors signature analysis as a medium for faults detection', *IEEE Trans. Ind. Electron.*, 2000, **47**, (5), pp. 984–993

[4] ARKAN M., PEROVIC D.K., UNSWORTH P.: 'Online stator fault diagnosis in induction motors', *IEE Proc. Electric Power Appl.*, 2001, **148**, (6), pp. 537–547

[5] WILLIAMSON S., SMITH A.C.: 'Steady-state analysis of 3-phase cage motors with rotor-bar and end-ring faults', *IEE Proc. B, Electr. Power Appl.*, 1982, **129**, (3), pp. 93–100

[6] BENBOUZID M.E.H., KLIMAN G.B.: 'What stator current processing-based technique to use for induction motor rotor faults diagnosis?', *IEEE Trans. Energy Convers.*, 2003, **18**, (2), pp. 238–244

[7] ELTABACH M., CHARARA A., ZEIN I.: 'A comparison of external and internal methods of signal spectral analysis for broken rotor bars detection in induction motors', *IEEE Trans. Ind. Electron.*, 2004, **51**, (1), pp. 107–121

[8] BELLINI A., FILIPPETTI F., TASSONI C., CAPOLINO G.A.: 'Advances in diagnostic techniques for induction machines', *IEEE Trans. Ind. Electron.*, 2008, **55**, (12), pp. 4109–4126

[9] BELLINI A., FILIPPETTI F., FRANCESCHINI G., TASSONI C.A., KLIMAN G.B.: 'Quantitative evaluation of induction motor broken bars by means of electrical signature analysis', *IEEE Trans. Ind. Appl.*, 2001, **37**, (5), pp. 1248–1255

[10] SCHOEN R.R., HABETLER T.G.: 'Effects of time-varying loads on rotor fault detection in induction machines', *IEEE Trans. Ind. Appl.*, 1995, **31**, (4), pp. 900–906

[11] BLODT M., BONACCI D., REGNIER J., CHABERT M., FAUCHER J.: 'On-line monitoring of mechanical faults in variable-speed induction motor drives using the Wigner distribution', *IEEE Trans. Ind. Electron.*, 2008, **55**, (2), pp. 522–533

[12] WU L., HABETLER T.G., HARLEY R.G.: 'A review of separating mechanical load effects from rotor faults detection in induction motors'. IEEE Int. Symp. on Diagnostics for Electric Machines, Power Electronics and Drives (SDEMPED), Cracow, Poland, September 2007, pp. 221–225

[13] DRIF M., BENOUZZA N., KRALOUA B., BENDIABDELLAH A., DENTE J.A.: 'Squirrel cage rotor faults detection in induction motor utilizing stator power spectrum approach'. Int. Conf. on Power Electronics, Machines and Drives (PEMD), University of Bath, UK, June 2002, pp. 133–138

[14] ALSHANDOLI A.F., BALL A.D., GU F.: 'Instantaneous phase variation (IPV) for rotor bar fault detection and diagnosis'. Second Int. Conf. on Electrical Engineering (ICEE), Lahore, Pakistan, March 2008, pp. 1–7

[15] CRUZ S.M.A., CARDOSO A.J.M.: 'Rotor cage fault diagnosis in three-phase induction motors by extended Park's vector approach', *Electr. Power Compon. Syst.*, 2000, **28**, (4), pp. 289–299

[16] MIRAFZAL B., DEMERDASH N.A.O.: 'On innovative methods of induction motor interturn and broken-bar fault diagnostics', *IEEE Trans. Ind. Appl.*, 2006, **42**, (2), pp. 405–414

[17] SCHOEN R.R., HABETLER T.G.: 'Evaluation and implementation of a system to eliminate arbitrary load effects in current-based monitoring of induction machines', *IEEE Trans. Ind. Appl.*, 1997, **33**, (6), pp. 1571–1577

[18] WU L., HABETLER T.G., HARLEY R.G.: 'Separating load torque oscillation and rotor fault effects in stator current-based motor condition monitoring'. IEEE Int. Conf. on Electric Machines and Drives (IEMDC), San Antonio, TX, USA, May 2005, pp. 1889–1894

[19] CRUZ S.M.A., CARDOSO A.J.M.: 'Rotor cage fault diagnosis in three-phase induction motors by the total instantaneous power spectral analysis'. Proc. IEEE Industry Applications Conf., 34th IAS Annual Meeting, Phoenix, AZ, USA, October 1999, vol. 3, pp. 1929–1934

[20] DRIF M., CARDOSO A.J.M.: 'The instantaneous reactive power approach for rotor cage fault diagnosis in induction motor drives'. IEEE Power Electronics Specialists Conf. (PESC), Rhodes, Greece, June 2008, pp. 1548–1552

[21] DRIF M., CARDOSO A.J.M.: 'Rotor cage fault diagnostics in three-phase induction motors, by the instantaneous phase-angle signature analysis'. IEEE Int. Electric Machines and Drives Conf. (IEMDC), Antalya, Turkey, May 2007, vol. 2, pp. 1440–1445

[22] DRIF M., MARQUES CARDOSO A.J.: 'On-line fault diagnostics in operating three-phase induction motors by the active and reactive power media'. 18th Int. Conf. on Electrical Machines (ICEM), Vilamoura, Portugal, September 2008, pp. 1–6

[23] DRIF M., MARQUES CARDOSO A.J.: 'Airgap eccentricity fault diagnosis, in three-phase induction motors, using the instantaneous power factor signature analysis'. Fourth IET Int. Conf. on Power Electronics, Machines and Drives (PEMD), York, UK, April 2008, pp. 587–591

[24] AKAGI H., KANAZAWA Y., NABAE A.: 'Generalized theory of the instantaneous reactive power in three-phase circuits'. IEEJ Int. Power Electronics Conf., Tokyo, 1983, pp. 1375–1386

[25] AKAGI H., WATANABE E.H., AREDES M.: 'Instantaneous power theory and applications to power conditioning' (Wiley-IEEE Press, 2007)

[26] BOSSIO G.R., DE ANGELO C.H., SOLSONA J.A., GARCÍA G.O., VALLA M.I.: 'Effects of rotor bar and end-ring faults over the signals of a position estimation strategy for induction motors', *IEEE Trans. Ind. Appl.*, 2005, **41**, (4), pp. 1005–1012

doi: 10.1049/iet-epa.2009.0101